

# L2RW+: A Comprehensive Benchmark Towards Privacy-Preserved Visible-Infrared Person Re-Identification

Yan Jiang, Hao Yu, Mengting Wei, Zhaodong Sun, Haoyu Chen, Xu Cheng, Guoying Zhao, *Fellow, IEEE*

**Abstract**—Visible-infrared person re-identification (VI-ReID) is a challenging task that aims to match pedestrian images captured under varying lighting conditions, which has drawn intensive research attention and achieved promising results. However, existing methods adopt the centralized training, ignoring the potential privacy concerns as the data is distributed across multiple devices or entities in reality. In this paper, we propose L2RW+, a benchmark that brings VI-ReID closer to real-world applications. The core rationale behind L2RW+ is that incorporating decentralized training into VI-ReID can address privacy concerns in scenarios with limited data-sharing constraints. Specifically, we design protocols and corresponding algorithms for different privacy sensitivity levels. In our new benchmark, we simulate the training under real-world data conditions that: 1) data from each camera is completely isolated, or 2) different data entities (e.g., data controllers of a certain region) can selectively share the data. In this way, we simulate scenarios with strict privacy restrictions, which is closer to real-world conditions. Comprehensive experiments show the feasibility and potential of decentralized VI-ReID training at both image and video levels. In particular, with increasing data scales, the performance gap between decentralized and centralized training decreases, especially in video-level VI-ReID. In unseen domains, decentralized training even achieves performance comparable to SOTA centralized methods. This work offers a novel research entry for deploying VI-ReID into real-world scenarios and can benefit the community. Code is available at: <https://github.com/Joey623/L2RW>.

**Index Terms**—Privacy-preserved, Visible-infrared, person re-identification.

## I. INTRODUCTION

THE growing need for reliable pedestrian identification throughout the day has made visible-infrared person re-identification (VI-ReID) a crucial technology [2]–[4]. It

An earlier version of this paper was presented at 2025 IEEE/CVF Conference on Computer Vision and Pattern Recognition (CVPR) [1].

This work was supported by the Research Council of Finland (former Academy of Finland) Academy Professor project EmotionAI (grants 336116, 359894), HPC project FaceCanvas (grant 364905), the University of Oulu & Research Council of Finland Profi 7 (grant 352788), the Finnish Doctoral Program Network in Artificial Intelligence, AI-DOC (grant VN/3137/2024-OKM-6), Academy Research Fellows Funding (grant 371019), the Startup Foundation for Introducing Talent of NUIST. As well, the authors wish to acknowledge CSC–IT Center for Science, Finland, for computational resources. Y.J. acknowledges the support of the China Scholarship Council program (Project ID: 202509040009). (Corresponding Author: Guoying Zhao)

Y. Jiang, H. Yu, M. Wei, H. Chen, G. Zhao is with Center for Machine Vision and Signal Analysis, University of Oulu, Oulu FI-90014, Finland (e-mail: yan.jiang@oulu.fi; hao.2.yu@oulu.fi; mengting.wei@oulu.fi; chen.haoyu@oulu.fi; guoying.zhao@oulu.fi)

Z. Sun and X. Cheng are with the School of Computer Science, Nanjing University of Information Science and Technology, Nanjing 210044, China (e-mail: zhaodong.sun@nuist.edu.cn; xcheng@nuist.edu.cn)

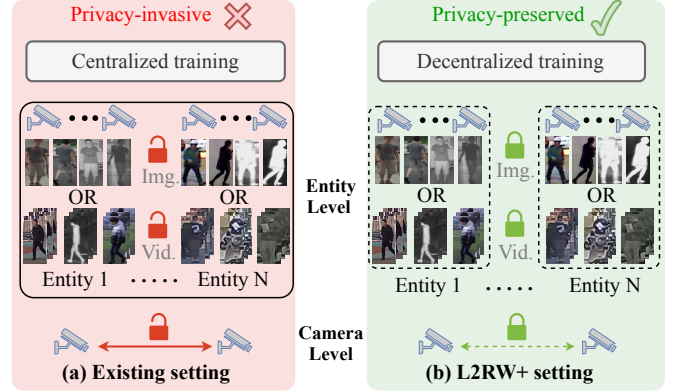


Fig. 1. Illustration of the existing setting and the proposed L2RW+ setting. (a) The existing setting relies on centralized training, allowing unrestricted data sharing between cameras or entities, which brings serious privacy concerns. Img. and Vid. denote the image and video, respectively. (b) Unlike this, our L2RW+ framework introduces camera-level and entity-level privacy regulation, simulating real-world privacy-preserved VI-ReID scenes. Our L2RW+ considers both image and video data, offering a comprehensive benchmark for VI-ReID.

solves the challenge of identifying individuals under varying lighting conditions, such as visible during the daytime and infrared at night. Although existing methods [5]–[12] have achieved encouraging advances, in our view, their settings are too idealized, thus restricting real-world deployments. To be specific, current VI-ReID methods adopt the centralized training, where data from multiple sources are aggregated on a central platform. Such settings overlook practical constraints such as privacy and data ownership, as surveillance data are typically distributed, sensitive, and subject to strict privacy restrictions, etc. This centralized training way in VI-ReID is overly idealized, and increases the risk of data leakage during the transmission of pedestrian images to the central server, bringing serious privacy concerns in real-world deployment.

To address this issue, our previous work presented L2RW [1] in CVPR2025, a benchmark that protects data privacy while still enabling effective VI-ReID. L2RW defined three protocols, i.e., Camera Independence (CI), Entity Independence (EI) and Entity Sharing (ES), to adapt to different privacy levels, thereby achieving flexible privacy level control. The definition of three protocols is shown in Tab. I. For CI, all camera data is isolated, which simulates the strictest privacy level where no data sharing occurs across every single camera as shown in the camera level of Fig. 1(b). Regarding a

TABLE I  
THE DETAILS OF THREE PROTOCOLS IN L2RW BENCHMARK.

Prot.	Description	Privacy
CI	All camera data is isolated	High
EI	Data is shared within an entity but isolated across entities	Medium
ES	All entity data is shared	Low

more relaxed privacy level in which all entity data is isolated while data can be shared inside each data entity, we propose the EI protocol as shown in the entity level of Fig. 1(b). When all data entities can be shared for centralized training, we name this protocol ES, as shown in Fig. 1(a), which is the commonly used protocol in previous Re-ID methods. In the ES protocol, existing VI-ReID methods [3], [13]–[16] can be seamlessly applied. However, these methods assume a closed-world setting where training and testing data come from the same entity, overlooking the domain generalization needed for open-world deployments. To address this, we evaluate generalization by training on multiple entities and testing on an unseen one under EI and ES protocols. Moreover, existing VI-ReID methods cannot be directly applied under these privacy-preserving protocols (CI and EI) due to *modality incomplete*, *identity missing*, and *domain shift* issues, as detailed in Sec. II-B. To solve this, our L2RW proposed the Image-based Decentralized Privacy-Preserved Training (I-DPPT), which employed decentralized training to ensure privacy protection while achieving VI-ReID. Generally, the contribution of L2RW can be summarized as follows: (1) We designed three protocols, i.e., CI (Camera Independence), EI (Entity Independence), and ES (Entity Sharing) to simulate scenarios with different privacy constraints; (2) We identified challenges under the CI and EI protocols, and proposed I-DPPT, the first decentralized VI-ReID method addressing privacy concerns; (3) Unlike existing methods evaluated on single datasets, our L2RW benchmark is the first work to merge multiple datasets for cross-domain evaluation. (4) Extensive experiments on three publicly available image-based VI-ReID datasets confirmed the feasibility of decentralized training in L2RW, with our method achieving significant improvement on various federated learning baselines under CI.

Despite these contributions, we argue that L2RW remains limited in two key aspects. First, L2RW only supports image data, whereas real-world surveillance systems predominantly collect continuous video streams rich in temporal and motion information, which cannot be processed by L2RW. Second, L2RW only demonstrates the feasibility and generalization ability of image-based VI-ReID, but lacks evaluation under real-world conditions such as environmental noise, adversarial attacks, and privacy leakage risks, leaving the model’s robustness and security largely unexplored.

To address these challenges, we propose L2RW+, an extension of L2RW that introduces the following improvements:

- From a methodology perspective, we extend decentralized VI-ReID from image-level to video-level and design Video-based Decentralized Privacy-Preserved Training (V-DPPT) for video data. V-DPPT effectively leverages temporal cues while respecting privacy constraints, en-

abling accurate retrieval from video data. L2RW+ unifies image and video evaluation under all three privacy protocols (CI, EI, ES). To the best of our knowledge, this is the first work that offers the comprehensive benchmark for privacy-preserved VI-ReID.

- From experiments, we demonstrate the feasibility and potential of decentralized training in VI-ReID. Specifically, under the CI protocol, our proposed DPPT shows the retrieval ability, even surpassing some methods trained under the centralized manner. Notably, the performance gap between decentralized and centralized training narrows on video data, suggesting that temporal information is useful for decentralized setups. Furthermore, under the EI and ES protocols, the model trained in a decentralized manner exhibits stronger generalization to unseen environments, especially when more training data becomes available. These findings not only validate the practical viability of decentralized learning in privacy-preserving VI-ReID but also emphasize the need for larger and more diverse VI-ReID datasets to better understand the consistent representation of visible and infrared modalities. Our L2RW+ offers meaningful insights and establishes a solid foundation for future privacy-preserved VI-ReID research.
- From a practical perspective, we show through extensive experiments that decentralized training is more robust than centralized training. In real-world VI-ReID applications, systems often face challenging conditions like rain, snow, or fog, and must also handle sensitive identity data that remains vulnerable to attacks. To reflect these challenges, we add noise to simulate harsh environments and apply various adversarial attacks. The results show that decentralized training maintains more stable performance and offers better privacy protection, as confirmed by gradient inversion experiments where pedestrian attributes are harder to recover.

Generally, this is the first work to introduce decentralized training into VI-ReID across both image and video data, showing superior performance on privacy, generalization, and robustness over centralized approaches. We believe our findings offer a practical and promising direction for deploying VI-ReID in real-world surveillance systems.

## II. RELATED WORK

### A. Visible-Infrared Person ReID

VI-ReID aims to match visible and infrared images of the same pedestrian captured by non-overlapping cameras. Many studies have emerged recently, achieving remarkable progress. Based on the input type, VI-ReID can be categorized into image-based and video-based subtasks.

**Image-based VI-ReID.** Zhang *et al.* [3] explored diverse modality-shared features to mine significant cross-modality patterns. Jiang *et al.* [16] designed domain shifting (DNS) that augments modality-specific and modality-shared representation, thereby regulating the model to concentrate on the consistency between modalities. Ren *et al.* proposed a novel implicit discriminative knowledge learning (IKDL) network

to discover identity-aware salient information for aligning visible and infrared modalities. Some auxiliary-based methods [6], [17], [18] have also been developed to achieve modality alignment with the help of generated auxiliary modalities. Feng *et al.* [17] proposed a shape-guided diverse feature learning framework (SGIEL) that employs the body shape as the auxiliary information for modality alignment. Yu *et al.* [6] proposed a modality unifying network (MUN) that constructed a robust auxiliary modality by intra- and inter-modality learners.

**Video-based VI-ReID.** Video-based VI-ReID aims to match pedestrian sequences across visible and infrared modalities. Different from image-based VI-ReID, it contains extra temporal information. Liu *et al.* [19] built the first video VI-ReID dataset dubbed HITSZ-VCM and designed the MITML method, attracting increasing research interest of this task. Specifically, Li *et al.* [20] designed an Intermediary-guided Bidirectional spatial-temporal Aggregation Network (IBAN) to mitigate the modality gap and learn the spatial-temporal representation by leveraging anaglyph data as the auxiliary. Du *et al.* [21] proposed AuxNet, which employs GANs for modality alignment and adopts a curriculum learning strategy to learn temporal information from the sequence, effectively reducing the cross-modality gap. Yu *et al.* [22] introduced TF-CLIP, which extracts identity-specific sequence features to replace the original text embeddings used in CLIP. Li *et al.* [23] introduced VLD that learned modality-invariant sequence-level pedestrian representations guided by video-level language prompts.

However, all the above methods are achieved under idealized lab settings, which neglect privacy constraints and heterogeneous environments that pose significant challenges in reality. More importantly, these methods require paired visible and infrared images, making privacy-preserved implementation infeasible, especially under CI, where modality information is unknown. In addition, existing works neglect the research on unseen environments, struggling to generalize effectively in real-world scenes. Therefore, we propose L2RW+, offering a novel, practical, and privacy-preserving benchmark for pushing VI-ReID closer to real world settings.

## B. Federated Learning

Federated Learning (FL) is a technology that enables multiple devices to collaborative learning without sharing private data. The pioneering work, FedAvg [24], averages the gradients of locally trained models and redistributes them to local clients for further training. Based on FedAvg, Li *et al.* [25] proposed FedProx, introducing a proximal term to ensure the convergence of the network in federated environments. Subsequently, Li *et al.* [26] designed MOON, which utilizes the modality representation similarity to correct the local training of clients. These methods brought new insights to the community, inspiring numerous impressive works that solve data heterogeneity [27]–[30] and model heterogeneity [31]–[33] in federated learning. This progress provides solid technical support for our L2RW+.

However, despite these advancements, existing FL methods are general methods and ignore the unique challenges arising

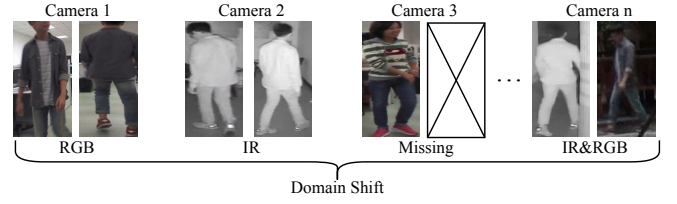


Fig. 2. Illustration of specific challenges in privacy-preserved VI-ReID. Each single camera may consist of only visible, only infrared, or both modalities, we name this modality incomplete. The pedestrian may not captured by all cameras or entities, which we define as identity missing. Data distribution is different across cameras/entities, inevitably resulting in domain shift.

from the heterogeneous and privacy-sensitive nature of VI-ReID data, as illustrated in Fig. 2. Let  $x$  and  $y$  denote the pedestrian images and their corresponding identity labels. Each client refers to an individual camera or data entity participating in decentralized training without data sharing. The main challenges include:

- **Domain shift:**  $P_i(x|y) \neq P_j(x|y)$ . Pedestrian images on different clients exhibit the non-iid (Independent and identically distributed) issue, where the corresponding feature distributions are different across different clients.
- **Modality incomplete:** For an individual client, pedestrian images can fall into three scenarios: only visible, only infrared, or both visible and infrared.
- **Identity missing:**  $P_i(y) \neq P_j(y)$ . The same subject might not appear in all cameras or entities.

To address these challenges, we propose two decentralized training frameworks: I-DPPT for image-based VI-ReID and V-DPPT for video-based VI-ReID. The DPPT is designed to work under privacy constraints and directly handle the problems of modality incompleteness, identity missing, and domain shift in federated settings. In addition, by adapting the model structure and training strategy to the characteristics of VI-ReID data, our approach achieves effective person retrieval without sharing data across clients.

## C. Domain Generalization

Domain generalization (DG) uses multiple seen domains to train a model that generalizes well to unseen domains. This technology aims to address the key issue of current deep learning methods, which heavily rely on the assumption that training and testing sets are independently and identically distributed. In practice, new information often arrives in continuous portions, leading to a domain gap between newly acquired data and the original data. This gap makes it challenging for the trained model to perform well on unseen data. Numerous works have emerged to extract domain-invariant features via contrastive loss [34]–[36], adversarial learning [37]–[39], causal learning [40]–[42], etc. Despite their success, these methods require centralized data from source domains and assume that data within the same domain shares the same distribution. These not only limit the applicability of these methods in decentralized settings but also increase the risk of privacy leakage.



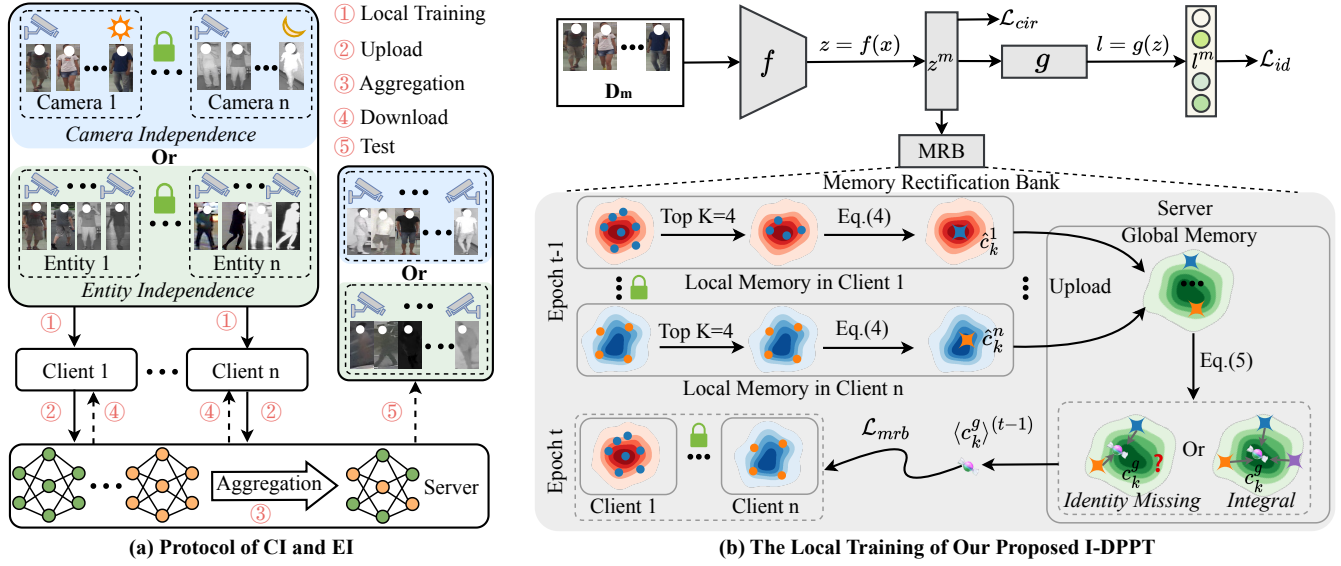


Fig. 3. Protocols and proposed method. (a) The protocols of camera independence (CI) and entity independence (EI) for privacy-preserved VI-ReID. Our proposed another protocol entity sharing (ES) is omitted in the figure, because its training way is the same as that used in existing VI-ReID methods. (b) The local training of our proposed image-based decentralized privacy-preserved training (I-DPPT). The local training of V-DPPT is shown in Fig. 4.

Conversely, our designed EI protocol in the L2RW+ benchmark eliminates the need to share source domain data, addressing privacy concerns. This also shows the feasibility of privacy domain generalization in VI-ReID and shows its potential for secure and effective deployment in reality.

### III. METHODOLOGY

In this section, we describe the proposed L2RW+ benchmark in detail. Sec. III-A presents the overview of the L2RW+. Then, three protocols we designed are elaborated in Sec. III-B, which are grounded in real-world scenarios: *camera independence* (CI), *entity independence* (EI), and *entity sharing* (ES). Finally, we introduce our proposed decentralized privacy-preserved training (DPPT) for image-based and video-based VI-ReID in Sec. III-C and Sec. III-D, respectively.

#### A. Overview

The overall pipeline of the L2RW+ benchmark is shown in Fig. 3(a). Let  $D_m = \{(x_i, y_i)\}_{i=1}^{N_m}$  denote the  $m$ -th local *image-level* private data, where  $x_i$  and  $y_i$  denote the pedestrian images and corresponding label, and  $N_m$  is the local data scale. The overall training set is denoted as  $D = \{D_1, D_2, \dots, D_n\}$ . In the realistic VI-ReID, each private dataset  $D_m$  can represent the data collected by a single camera or the surveillance data from within a specific entity. The overall process of the L2RW+ can be roughly summarized into five steps. ① **Local Training**: Each private data is trained by a local model  $\theta^l$  (client). ② **Upload**: Each client model weight is uploaded to the server. ③ **Aggregation**: The uploaded local model weights are aggregated to obtain the global model weight  $\theta^g$ . ④ **Download**: The global model weight  $\theta^g$  is downloaded by the clients for next local training. By repeating step ① to ④ until convergence, execute ⑤ **Test**: test seen domains or unseen domains according to the protocol.

#### B. Benchmark Protocols

Considering real-world conditions, we design three protocols, i.e., *camera independence* (CI), *entity independence* (EI), and *entity sharing* (ES), to simulate different privacy-restricted scenarios.

**Protocol 1: Camera Independence (CI)**: *all camera data remains isolated, which simulates the most strict setting where no data sharing occurs across every single device.*

It solves the concerns about data privacy, ownership regulations, or security policies in reality. However, existing VI-ReID methods cannot be directly applied under CI due to the *modality incomplete* issue. Specifically, current VI-ReID methods require paired visible and infrared images of the same identity as input during training, which is achieved through the *PK* strategy.  $P$  identities with  $K$  visible and  $K$  infrared images are randomly sampled from the training set (i.e., mini-batch =  $2 \times P \times K$ ). These methods typically use a dual-stream architecture to extract modality-specific features in the shallow layers and modality-shared features in the deeper layers, relying on modality information as a prerequisite. However, under the CI protocol, the modality information is unknown, as each camera may contain only visible, only infrared, or both modalities. This modality incomplete issue makes existing VI-ReID methods incompatible with the CI protocol.

To solve these issues, we convert the two-stream structure into a one-stream architecture and only sample images according to identity rather than identity and modality. Specifically, we randomly sample  $K$  images from  $P$  identities in the  $m$ -th local private data  $D_m$ , where the  $K$  images can be visible, infrared, or a mix of both. This eliminates the reliance on the paired visible and infrared images of the same subject as the input, thereby addressing the *modality incomplete*. In addition, we also employ channel augmentation (CA) [14] by randomly selecting one channel (R, G, or B) to replace the other two



channels, which reduces the cross-modality gap across clients.

**Protocol 2&3: Entity Independence and Entity Sharing (EI&ES).**

In real-world scenarios, it is often feasible for an entity (data controller) to access all data within its designated region or with other data entities, which is a more relaxed privacy regulation compared to CI. Therefore, based on varying levels of mutual trust and privacy agreements, we categorize entity-level privacy regulation into two protocols: **Entity Independence (EI)** and **Entity Sharing (ES)**.

**EI:** *Data from different entities is kept isolated during training, and the model is trained using a decentralized way. Then the trained model is evaluated on an unseen entity to assess its generalization ability.*

EI ensures that data sharing across entities is entirely avoided, aligning with real-world privacy requirements and ensuring data security. It also guarantees that knowledge is still transferred across entities without exposing raw data, providing a practical and secure solution for VI-ReID in real-world deployments.

**ES:** *Data from different entities is shared during training, and the model is evaluated on an unseen entity to assess its generalization ability.*

In such an ES protocol, existing VI-ReID methods can be seamlessly applied. However, note that these methods' evaluation protocols are often designed on the same dataset, where the data distribution is assumed to be consistent. Meanwhile, in our ES protocol, we merge several existing datasets and conduct the evaluation in a cross-domain manner to simulate real-world scenarios. To the best of our knowledge, this has not been explored before and remains an open issue.

We reproduce several VI-ReID methods [3], [13]–[16] under this protocol, which will be discussed in Sec. IV-C. Additionally, we provide a baseline using Empirical Risk Minimization (ERM) [43]. It merges data from all training domains to learn domain-invariant knowledge and can be formulated as follows:

$$\mathcal{L}_{ERM} = \min_{f,g} \frac{1}{|\mathcal{V}|} \sum_{V_i \in \mathcal{V}} \mathcal{R}^{V_i}(f, g), \quad (1)$$

where  $f$  and  $g$  are the encoder and classifier, respectively.  $V_i$  is the  $i$ -th entity, and  $\mathcal{V}$  is a set containing all entities. The empirical risk function  $\mathcal{R}^{V_i}(f, g)$  for a given entity  $V_i$  is defined by:

$$\mathcal{R}^{V_i}(f, g) \triangleq \mathbb{E}_{(x_j, y_j) \sim V_i} \mathcal{L}((x_j; f, g), y_j), \quad (2)$$

where our baseline loss function  $\mathcal{L}(\cdot, \cdot)$  includes the identity loss and circle loss. It is worth noting that this protocol is fully compatible with existing methods designed for laboratory settings, as it does not change their training paradigm. The loss function  $\mathcal{L}(\cdot, \cdot)$  can be replaced with the specific loss functions employed by those methods, ensuring seamless integration with their frameworks. Our protocol provides a fair and comprehensive evaluation of the generalization capability of existing VI-ReID approaches.

### C. Image-based Decentralized Privacy-Preserved Training

To address the challenges in CI and EI, we propose the image-based decentralized privacy-preserved training (I-

DPPT) for image data. I-DPPT consists of five steps aimed at addressing the challenges encountered in these protocols that cannot be effectively resolved through existing VI-ReID methods. We will introduce one by one.

① **Local Training:** The process of client local training is shown in Fig. 3(b). The private data are fed into the encoder and get the  $l_2$ -normalized feature embedding  $z$  and logits  $l$ . The identity loss  $\mathcal{L}_{id}$  and circle loss  $\mathcal{L}_{cir}$  are employed as the baseline loss functions (provided in the supplementary material) to ensure the learned features and logits are identity-related. However, this training objective design cannot address the domain shift and identity missing, as the model tends to overfit the current private data in the client training and forget previously learned knowledge after download. Driven by this, we propose a memory rectification bank (MRB) that enables different clients to optimize towards the same goal.

**MRB.** Specifically, we design a local memory  $\mathcal{M}^l$  to store  $l_2$ -normalized feature embedding  $z$  in each client. We first calculate the mean vector  $c_k$  that store features belonging to the same class via Eq. 3:

$$c_k^m = \frac{1}{|S_k^m|} \sum_{(z_i^m, y_i^m) \in S_k^m} z_i^m, \quad (3)$$

where  $S_k^m$  denotes the set of samples annotated with class  $k$  in the  $m$ -th client. The local memory can be denoted as  $\mathcal{M}_m^l = \{c_1^m, c_2^m, \dots, c_{I_m}^m\}$ . Each center can be viewed as a representative of each identity, containing client-specific information. By aggregating the center from different clients, a representative encompassing all clients can be obtained without leaking the original data. However, the modality and number of images for each pedestrian within a camera are unknown, and the centers for different individuals are generated from varying sample numbers, which undermines fairness between identities. Additionally, images affected by occlusions or environmental interference contain lower semantic information, which can distort the center calculation. Therefore, our MRB adjusts the centers by averaging the top  $K$  closest feature embeddings to the center, effectively filtering out low-information features and providing a fairer representation for each identity. It is defined as:

$$\hat{c}_k^m = \begin{cases} c_k^m, & \text{if } |S_k^m| < K, \\ \frac{1}{K} \sum \min_K d(z_i^m, c_k^m), & \text{if } |S_k^m| \geq K, \end{cases} \quad (4)$$

where  $d(\cdot, \cdot)$  is the Euclidean distance and the local memory is updated as  $\mathcal{M}_m^l = \{\hat{c}_1^m, \hat{c}_2^m, \dots, \hat{c}_{I_m}^m\}$ ,  $I_m$  is the identity number in client  $m$ . The local memory is uploaded to the server and aggregated through a global memory  $\mathcal{M}^g$ , as defined below:

$$\mathcal{M}^g = \left\{ \hat{c}_i^g = \frac{\sum_{m=1}^n \mathbb{1}_{\{\hat{c}_i^m \neq 0\}} \cdot \hat{c}_i^m}{\sum_{m=1}^n \mathbb{1}_{\{\hat{c}_i^m \neq 0\}}} \middle| i = 1, 2, \dots, I \right\}, \quad (5)$$

where  $n$  is the number of clients.  $I$  is the total identity number, and  $I_m \leq I$ , thereby handling the *identity missing* issue.  $\mathbb{1}$  denotes the indicator function. The global memory contains information from different domains while ensuring no data leakage. In the next round of local training, we use the memory

rectification bank loss  $\mathcal{L}_{mrb}$  to guide the optimization of the locally updated memory towards the global memory, thereby relieving domain shift. The  $\mathcal{L}_{mrb}$  is defined as follows:

$$\mathcal{L}_{mrb} = \frac{1}{N_m} \sum_{i=1}^{N_m} \left( 1 - \frac{\langle z_i^m \rangle^{(t)} \cdot \langle c_{y_i}^g \rangle^{(t-1)}}{\|\langle z_i^m \rangle^{(t)}\| \times \|\langle c_{y_i}^g \rangle^{(t-1)}\|} \right), \quad (6)$$

where  $\langle z_i^m \rangle^{(t)}$  is the  $i$ -th  $l_2$ -normalized feature embedding in the  $t$ -th epoch on the  $m$ -th client.  $\langle c_{y_i}^g \rangle^{(t-1)}$  is the global center of identity  $y_i$  in the last epoch  $t-1$ , which contains the knowledge from the client  $m$  and the other clients without leaking raw data.  $\mathcal{L}_{mrb}$  pulls together the local memory and the global memory, addressing the domain shift and identity missing. The total training loss of the  $m$ -th client can be written as:

$$\mathcal{L}_{all} = \mathcal{L}_{id} + \mathcal{L}_{cir} + \lambda \mathcal{L}_{mrb}, \quad (7)$$

where  $\lambda$  is the loss balance factor.

② **Upload:** The client model parameters  $\theta^l$  are upload to the server, denoted by  $\{\theta_1^l, \dots, \theta_n^l\}$ .

③ **Aggregation:** The uploaded local model parameters are aggregated to obtain the global model parameters  $\theta^g$ :

$$\theta^g = \sum_{i=1}^n \frac{N_i}{N_{total}} \theta_i^l, \quad (8)$$

where  $N_{total} = \sum_{i=1}^n N_i$  is the total number of samples across all clients.

④ **Download:** The global model parameters  $\theta^g$  is downloaded by the clients for next local training.

⑤ **Test:** After training, test seen domains or unseen domains according to the CI or EI protocols. The overall process is shown in Algorithm 1.

#### D. Video-based Decentralized Privacy-Preserved Training

Unlike image-based VI-ReID, video-based VI-ReID takes as input a sequence of tracklets corresponding to each subject, which inherently contains temporal information. Within a tracklet, the same person may exhibit different poses over time, and different individuals often have distinct walking patterns and styles. As a result, video-based VI-ReID is more challenging than its image-based counterpart, as it requires addressing not only cross-modality and intra-modality variations but also learning temporal-invariant representations. Since our approach is the first to consider VI-ReID in a realistic, video-based setting, we aim to make minimal modifications to existing image-based methods to enable their seamless adaptation to video-based VI-ReID. Therefore, we only modify the local training stage, keeping other settings (including the proposed MRB) identical to image-based VI-ReID. We name it video-based decentralized privacy-preserved training (V-DPPT), and the details are illustrated in Fig. 4.

Specifically, let  $D_m^{video} = \{(X_i, y_i)\}_{i=1}^{N_m}$  denote the  $m$ -th local video-level private data, where  $X_i \in \mathbb{R}^{T \times H \times W \times C}$  and  $y_i$  denote the pedestrian videos and corresponding label, and  $N_m$  is the local data scale. The input is fed into the encoder to get the  $l_2$ -normalized feature embedding  $z^t$ . Then we average

#### Algorithm 1: I-DPPT

---

**Input:** Number of clients  $n$ ; initial global model  $\theta^g$ ; local models  $\{\theta_1^l, \dots, \theta_n^l\}$ ; datasets  $\{D_1, \dots, D_n\}$ ; number of epochs  $E$

**Output:** Final global model  $\theta^g$  for test

**for**  $e = 1$  **to**  $E$  **do**

**for**  $m = 1$  **to**  $n$  **do**

$\theta_m^l, \mathcal{M}_m^l \leftarrow \text{ClientTraining}(\theta^g, D_m, \mathcal{M}^g)$

**end**

// Upload and aggregate the local models

$\theta^g \leftarrow \sum_{i=1}^n \frac{|D_i|}{\sum_{j=1}^n |D_j|} \theta_i^l$

// Upload and aggregate the local memory banks

$\mathcal{M}^g \leftarrow \{c_i^g = \frac{\sum_{m=1}^n \mathbb{1}_{\{c_i^m \neq 0\}} \cdot c_i^m}{\sum_{m=1}^n \mathbb{1}_{\{c_i^m \neq 0\}}} \mid i = 1, 2, \dots, I\}$

**end**

**ClientTraining** $(\theta^g, D_m, \mathcal{M}^g)$ :

$\theta_m^l \leftarrow \theta^g$  // Download the global model

**for**  $(x_i, y_i) \in D_m$  **do**

$z_i = f_m(x_i), l_i = g_m(z_i)$

$\mathcal{L}_{cir} \leftarrow (z_i, y_i), \mathcal{L}_{id} \leftarrow (l_i, y_i)$

Update  $\mathcal{M}_m^l$  with  $z_i$  via Eq.(3, 4)

$\mathcal{L}_{mrb} \leftarrow (\mathcal{M}_m^l, \mathcal{M}^g)$  via Eq.(6)

$\mathcal{L} = \mathcal{L}_{id} + \mathcal{L}_{cir} + \lambda \mathcal{L}_{mrb}$

$\theta_m^l \leftarrow \theta_m^l - \eta \nabla \mathcal{L}$

**end**

**return**  $\theta_m^l, \mathcal{M}_m^l$

---

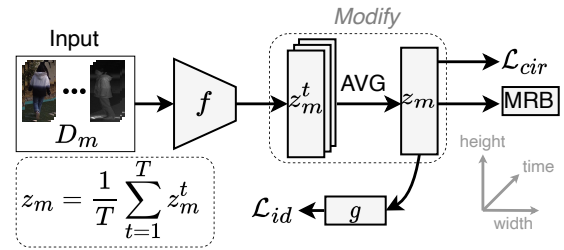


Fig. 4. The local training of our proposed video-based decentralized privacy-preserved training (V-DPPT).

the  $z^t$  along the time dimension to obtain the temporal-level representation, as defined below:

$$z_m = \frac{1}{T} \sum_{t=1}^T z_m^t, \quad (9)$$

where  $T$  denotes the total number of images in the sequence. Then  $z$  is input to the classifier and the proposed MRB. Finally, the identity loss  $\mathcal{L}_{id}$ , circle loss  $\mathcal{L}_{cir}$ , and the proposed memory rectification bank loss  $\mathcal{L}_{MRB}$  are employed to optimize the whole training stage.

It should be noted that, unlike image-based VI-ReID, the fundamental unit of video-based VI-ReID is a pedestrian sequence rather than an individual image. Consequently, the mini-batch construction is different from image-based VI-ReID. Specifically, we randomly sample  $K$  sequences from

$P$  identities in the  $m$ -th local private data  $D_m^{video}$ . There is a total of  $K \times P \times T$  images in each mini-batch, where  $T$  is the total number of images in the sequence. The modality information of each sequence is unknown, but all images within a sequence have the same modality. Besides this, all the settings are identical to the image-based VI-ReID.

#### IV. EXPERIMENTS

##### A. Datasets and Evaluation Metrics

**Datasets.** We conduct experiments on five widely used VI-ReID datasets to evaluate our proposed method. Three of them are image datasets, i.e., SYSU-MM01 [2], RegDB [44], and LLCM [3]. The remaining two are video datasets, i.e., HITSZ-VCM [19] and BUPTCampus [21].

**SYSU-MM01** [2] contains 44,754 images of 491 identities captured by four visible and two infrared cameras, including 29,033 visible images and 15,715 infrared images. **RegDB** [44] contains 412 identities collected by one visible and one infrared camera. Each identity has 10 visible and 10 infrared images. **LLCM** [3] contains 46,767 images of 1,064 identities captured by 9 visible and infrared cameras, with the training and testing sets split at an approximate ratio of 2:1. **HITSZ-VCM** [19] contain 927 identities captured by six cameras. Every 24 consecutive images in a video are regarded as a tracklet for a person during the same period. There are 251,452 visible images and 211,807 infrared images in total, which can be divided into 11,785 and 10,078 tracklets, respectively. 500 identities are used as the training set, and the remaining 427 identities are used as the testing set. **BUPTCampus** [21] contains 3,080 identities and 16,826 video tracklets, divided into 1,074 identities for primary learning, 930 for auxiliary learning, and 1,076 for testing. In our experiments, we exclude the auxiliary identities.

**Evaluation Metrics.** Following existing VI-ReID settings [3], we adopt the rank- $k$  matching accuracy, mean Average Precision (mAP), and mean Inverse Negative Precision (mINP) [13] as evaluation metrics. The protocols in terms of CI, EI, and ES are defined in Sec. III-B. Following [2], [3], [13], [14], [16], [19], [21], all datasets are used in infrared-to-visible mode for clarity, where infrared images serve as the query set, and visible images as the gallery.

##### B. Implementation Details

We adopt the ResNet-50 [48] pretrained on the ImageNet-1k [49] as our backbone. During the training state, all the input images are resized to  $288 \times 144$ . For image-based VI-ReID, the batch size is set to 64, where eight identities with eight images are randomly sampled. For VCM, the batch size is set to 64, where similarly eight identities with eight sequences are randomly sampled. The sequence length  $T$  is set to 6 following the official [19]. For BUPTCampus, the batch size is set to 16, where 16 identities with one sequence are randomly sampled. The sequence length  $T$  is set to 10 in accordance with the official setting [21]. The Stochastic Gradient Descent (SGD) optimizer is adopted, with a weight decay of  $5e^{-4}$  and momentum of 0.9. The initial learning rate is set to 0.2, and the OneCycleLR scheduler [50] is adopted. The number of epochs

for CI and EI experiments is set to 50 and 30 for image-level settings, respectively, and 100 for video-level settings. The FedAvg [24] is employed as our default. The TOP  $K = 4$  and  $\lambda = 1$  are decided by ablations on settings.

For CI, each client model is trained using data from a single camera within the training set of a given dataset. The global model is then evaluated on the testing set of the same dataset. For EI under image-level VI-ReID, we have two client models. Two datasets (entities) are used to train the two client models, respectively, and another new entity is used to test the global model. For ES, which is similar to EI, two entities are merged to train a model, and the model is tested on a new entity, which is not learned during training. Due to the limited video-based VI-ReID datasets, the EI protocol cannot be directly implemented. Instead, we use the model weights trained under the CI protocol for direct testing on other unseen datasets. For the video-based VI-ReID ES protocol, we reproduce several video-based VI-ReID methods by training them on one dataset and directly evaluating them on another unseen dataset.

##### C. Quantitative Analysis for Image-based VI-ReID

**Evaluation on the CI Protocol.** The results are reported on Tab. II. It is noted that existing VI-ReID methods require paired visible and infrared images as input, making them unsuitable for addressing the modality incomplete challenge under the CI protocol. Therefore, we report our results using four classic federated learning algorithms: FedProx [25], Fednova [45], Moon [26], and FedAvg [24], each adopting different aggregation strategies. For these methods, the setting of local training is the same, conducting ResNet-50 supervised by  $\mathcal{L}_{id}$  and  $\mathcal{L}_{cir}$ . The comparison methods after + only modify the local training stage, with all other steps remaining consistent. The compared method only changes the local training stage. It is obvious that our proposed I-DPPT achieves consistent improvements across the board. Additionally, we modify two VI-ReID methods, i.e., AGW [13] and DNS [16], by converting their two-stream architecture into a single-stream structure, adopting our proposed sampling approach, and removing their modality information (denoted by AGW<sup>†</sup> and DNS<sup>†</sup>). They remain a significant performance gap compared with our DPPT.

Furthermore, we compare our proposed I-DPPT with existing VI-ReID methods based on centralized training, as shown in Tab. III. It can be observed that a noticeable performance gap remains between decentralized and centralized training approaches. This can be attributed to two main factors. First, centralized methods typically have access to modality and camera information; Second, they often incorporate additional modules and loss functions to alleviate the cross-modality gap. However, we observe that as the amount of training data increases, the gap between decentralized training and the best centralized methods consistently narrows. To be specific, the three datasets, namely RegDB, SYSU-MM01, and LLCM, are listed in ascending order of training data size. The rank-1 accuracy gaps between our method and the best-performing centralized methods (marked underline in table) on these datasets are 34.15%, 26.53%, and 22.76%, respectively.



TABLE II

EVALUATION OF OUR I-DPPT UNDER CI PROTOCOL (BEST RESULTS IN BOLD). *Note that existing VI-ReID methods cannot be directly applied to the CI protocol as their frameworks are designed for data-shared learning.* THUS, WE IMPLEMENTED FOUR CLASSIC FEDERATED LEARNING ALGORITHMS AS BASELINES TO VERIFY THE EFFICACY OF OUR METHOD: FEDPROX [25], FEDNOVA [45], MOON [26], AND FEDAVG [24]. EVALUATING METRICS RANK-1(%), RANK-10(%), MAP(%), AND MINP(%) ARE REPORTED. AGW<sup>†</sup> AND DNS<sup>†</sup> ARE THE REPRODUCED VI-ReID METHOD THAT REMOVES THE MODALITY INFORMATION.

Methods	SYSU-MM01 [2] (Image)				RegDB [44] (Image)				LLCM [3] (Image)			
	r=1 ↑	r=10 ↑	mAP ↑	mINP ↑	r=1 ↑	r=10 ↑	mAP ↑	mINP ↑	r=1 ↑	r=10 ↑	mAP ↑	mINP ↑
FedProx [25]	25.90	68.83	27.48	17.18	25.62	44.19	25.96	17.80	23.72	53.95	30.59	27.69
+AGW <sup>†</sup> [13]	21.50	62.59	23.07	13.89	20.82	38.94	21.57	14.35	24.65	55.98	31.62	28.45
+DNS <sup>†</sup> [16]	36.11	78.29	35.22	22.02	46.75	69.27	43.06	28.99	26.35	57.00	32.88	29.54
+I-DPPT (Ours)	<b>38.16</b>	<b>81.54</b>	<b>38.15</b>	<b>25.17</b>	<b>51.33</b>	<b>71.43</b>	<b>48.93</b>	<b>36.15</b>	<b>27.46</b>	<b>59.33</b>	<b>34.60</b>	<b>31.44</b>
Fednova [45]	29.15	74.00	31.34	20.77	20.50	35.00	22.15	16.41	-	-	-	-
+AGW <sup>†</sup> [13]	22.00	64.15	23.52	13.54	13.83	25.47	15.92	12.21	-	-	-	-
+DNS <sup>†</sup> [16]	40.79	83.14	41.01	27.87	46.70	68.15	43.40	29.92	-	-	-	-
+I-DPPT (Ours)	<b>50.37</b>	<b>88.92</b>	<b>48.67</b>	<b>33.65</b>	<b>59.67</b>	<b>78.36</b>	<b>55.17</b>	<b>41.12</b>	-	-	-	-
Moon [26]	26.88	71.65	29.54	19.55	19.96	34.19	21.54	15.93	25.02	57.58	32.34	29.25
+AGW <sup>†</sup> [13]	20.79	62.57	22.44	12.80	11.19	20.56	13.44	10.46	23.60	55.98	31.62	28.45
+DNS <sup>†</sup> [16]	38.18	81.31	38.94	26.53	43.60	65.46	40.33	27.87	29.55	60.82	36.64	33.52
+I-DPPT (Ours)	<b>46.78</b>	<b>87.40</b>	<b>45.99</b>	<b>31.74</b>	<b>53.22</b>	<b>73.01</b>	<b>49.27</b>	<b>35.46</b>	<b>32.66</b>	<b>64.83</b>	<b>39.78</b>	<b>36.41</b>
FedAvg [24]	27.51	72.26	29.98	19.79	19.07	32.95	21.05	15.61	26.24	59.31	33.52	30.24
+AGW <sup>†</sup> [13]	21.65	63.13	23.25	13.45	14.17	23.84	15.89	12.10	24.31	54.51	30.66	27.19
+DNS <sup>†</sup> [16]	39.60	81.96	40.09	27.64	48.48	69.76	45.30	31.51	30.79	62.29	37.81	34.66
+I-DPPT (Ours)	<b>51.27</b>	<b>88.55</b>	<b>49.29</b>	<b>34.47</b>	<b>59.85</b>	<b>77.58</b>	<b>55.58</b>	<b>41.70</b>	<b>34.69</b>	<b>67.20</b>	<b>41.91</b>	<b>38.48</b>

TABLE III

COMPARISON WITH RECENT VI-ReID METHODS BASED ON CENTRALIZED TRAINING. ALL THE COMPARED METHODS ARE THE CENTRALIZED TRAINING METHOD, BUT OUR I-DPPT ADOPTS THE DECENTRALIZED TRAINING. THE UNDERLINED INDICATE THE BEST RESULTS FOR THE EXISTING CENTRALIZED TRAINING VI-ReID METHODS.  $\Delta$  DENOTE THE RETRIEVAL ACCURACY GAP BETWEEN OUR I-DPPT AND THE EXISTING BEST CENTRALIZED METHOD.

Methods	Venue	SYSU-MM01		RegDB		LLCM	
		r=1 ↑	mAP ↑	r=1 ↑	mAP ↑	r=1 ↑	mAP ↑
DEEN [3]	CVPR23	74.70	71.80	89.50	83.40	56.60	62.70
HOSNet [46]	AAAI24	75.60	74.20	93.30	<u>89.20</u>	56.40	63.20
DSAF [47]	TMM25	76.65	73.24	92.62	86.37	57.34	<u>64.27</u>
DSF [16]	ECCV24	77.27	74.35	93.49	88.10	<u>57.45</u>	64.11
FDMN [7]	TIFS25	<u>77.80</u>	<u>75.10</u>	<u>94.00</u>	88.70	56.60	62.70
I-DPPT	-	<b>51.27</b>	<b>49.29</b>	<b>59.85</b>	<b>55.58</b>	<b>34.69</b>	<b>41.91</b>
$\Delta$	-	26.53	25.81	34.15	33.62	22.76	22.36

Considering that surveillance systems in real-world scenarios typically capture massive volumes of pedestrian data, these observations are encouraging and suggest strong potential for the practical adoption of decentralized training approaches in VI-ReID.

**Evaluation on ES and EI Protocols.** We first replicate several recent VI-ReID methods [3], [13]–[16] to evaluate their generalization ability under the ES protocol, shown in Tab. IV. While most methods slightly outperform our baseline B (ERM with  $\mathcal{L}_{id}$  and  $\mathcal{L}_{cir}$ ), the differences are minimal, and overall rank-1 accuracy remains low. This suggests that current VI-ReID methods still have limited capability in handling unseen environments. We encourage researchers to explore the bottlenecks that limit the generalization ability of existing methods, bringing VI-ReID closer to the real world and advancing the community. Moreover, we report our method under the EI protocol. Remarkably, our I-DPPT achieves comparable or even superior performance under EI compared to methods evaluated under ES. Moreover, the baseline results under the EI protocol ( $B^{\dagger}$ ) are similar to those under the ES protocol (B), indicating that decentralized training does not significantly impact the model’s ability to generalize to unseen

environments.

#### D. Quantitative Analysis for Video-based VI-ReID

**Evaluation on the CI Protocol.** As shown in Tab. II, we reproduce four classic FL algorithms [24]–[26], [45] for image-level VI-ReID and find that methods proposed after FedAvg even perform worse than FedAvg under the CI protocol. *The reason is that these FL methods are general methods and ignore the unique challenges of VI-ReID. Therefore, we did not reproduce additional FL methods and adopted FedAvg as our default.* The results are reported in Table V. Similar to prior work, existing video-based VI-ReID methods are not directly applicable under the CI protocol since their frameworks rely on centralized data access. Therefore, we compare our proposed approach under the CI setting with methods that use centralized training. Although there remains a noticeable gap from the current state-of-the-art, the performance difference is gradually narrowing, particularly when compared to image-based VI-ReID methods. Notably, our method achieves a rank-10 accuracy of 79%, indicating that the correct target appears within the top 10 retrieved sequences with a 79% probability. This substantially reduces the need for manual verification and demonstrates the practical utility of our method in real-world applications.

Moreover, *it can be observed that the performance gap between decentralized and centralized training methods is smaller on video datasets compared to image datasets.* Specifically, our DPPT exhibits a rank-1 gap of 15.97% with VLD on the HITSZ-VCM dataset, and 17.24% with DNS on the BUPTCampus dataset. The potential reason is that video datasets consist of sequences of pedestrian frames, where variations in background and lighting conditions are relatively limited. This consistency facilitates learning identity-preserving representations and leads to improved robustness in handling cross-modality discrepancies. Additionally, the training set of HITSZ-VCM is larger than that of BUPTCampus, and correspondingly, the gap with the best method is smaller,

TABLE IV

EVALUATION OF OUR I-DPPT UNDER EI AND ES PROTOCOLS. THE UPPER PART OF THE TABLE IS UNDER ES, WHILE THE LOWER PART IS UNDER EI. THE UNDERLINED AND BOLD INDICATE THE BEST RESULTS FOR BOTH PROTOCOLS, RESPECTIVELY. B IS THE BASELINE USING ERM WITH  $\mathcal{L}_{id}$  AND  $\mathcal{L}_{cir}$  UNDER ES, B<sup>†</sup> DENOTE THE BASELINE USING FEDAVG SUPERVISED BY  $\mathcal{L}_{id}$  AND  $\mathcal{L}_{cir}$  UNDER EI. WE USE R, L, AND S TO DENOTE REGDB, LLCM, AND SYSU-MM01 DATASETS, RESPECTIVELY. THE LEFT OF  $\rightarrow$  INDICATES SEEN ENTITIES, AND THE RIGHT IS THE UNSEEN ENTITY.

Methods	Prot.	FLOPs	R [44] + L [3] $\rightarrow$ S [2] (Image)				L [3] + S [2] $\rightarrow$ R [44] (Image)				R [44] + S [2] $\rightarrow$ L [3] (Image)			
			r=1 $\uparrow$	r=10 $\uparrow$	mAP $\uparrow$	mINP $\uparrow$	r=1 $\uparrow$	r=10 $\uparrow$	mAP $\uparrow$	mINP $\uparrow$	r=1 $\uparrow$	r=10 $\uparrow$	mAP $\uparrow$	mINP $\uparrow$
B	ES	10.34	8.63	36.26	9.57	4.01	17.08	34.32	17.69	11.15	8.74	26.83	12.23	9.78
LBA [15]	ES	10.36	8.09	34.63	9.55	4.29	12.01	28.65	11.69	6.01	8.38	26.80	12.20	9.90
AGW [13]	ES	10.36	9.59	38.28	10.42	4.45	13.79	29.76	14.05	8.25	9.08	26.77	12.37	9.80
DEEN [3]	ES	27.70	9.48	38.39	10.03	3.72	<u>19.42</u>	37.59	<u>19.44</u>	<u>12.33</u>	10.50	29.41	14.09	11.48
CAJ [14]	ES	10.36	10.90	40.57	11.18	4.39	16.55	37.23	17.40	10.74	<u>11.35</u>	<u>31.17</u>	<u>15.03</u>	<u>12.10</u>
DNS [16]	ES	10.36	<u>11.75</u>	<u>42.36</u>	<u>11.77</u>	<u>4.56</u>	18.87	<u>37.79</u>	18.36	10.56	10.14	28.47	13.55	10.94
B <sup>†</sup>	EI	5.17	9.72	38.21	10.74	4.75	15.37	29.95	16.77	10.90	8.97	26.81	12.85	10.62
B <sup>†</sup> +CA	EI	5.17	10.10	39.34	10.73	4.19	17.61	33.58	17.73	11.31	14.40	35.87	18.89	16.30
I-DPPT (Ours)	EI	5.17	<b>11.27</b>	<b>41.20</b>	<b>11.86</b>	<b>5.34</b>	<b>21.54</b>	<b>40.37</b>	<b>20.72</b>	<b>12.78</b>	<b>14.63</b>	<b>37.03</b>	<b>19.15</b>	<b>16.44</b>

TABLE V

EVALUATION OF OUR V-DPPT UNDER CI PROTOCOL. FROM TAB. II WE CAN FIND THAT METHODS PROPOSED AFTER FEDAVG EVEN PERFORM WORSE THAN FEDAVG UNDER THE CI PROTOCOL. THE REASON IS THAT THESE FL METHODS ARE GENERAL METHODS AND IGNORE THE UNIQUE CHALLENGES OF VI-ReID. THEREFORE, WE DID NOT REPRODUCE ADDITIONAL FL METHODS AND ADOPTED FEDAVG AS OUR DEFAULT. THE UPPER PART OF THE TABLE LISTS METHODS BASED ON CENTRALIZED TRAINING, WHILE THE LOWER PART IS OUR PROPOSED METHODS BASED ON DECENTRALIZED TRAINING.  $\Delta$  DENOTE THE RETRIEVAL ACCURACY GAP BETWEEN OUR V-DPPT AND THE EXISTING BEST CENTRALIZED METHOD.

Methods	Venue	HITSZ-VCM [19] (Video)						BUPTCampus [21] (Video)					
		r=1 $\uparrow$	r=5 $\uparrow$	r=10 $\uparrow$	r=20 $\uparrow$	mAP $\uparrow$	mINP $\uparrow$	r=1 $\uparrow$	r=5 $\uparrow$	r=10 $\uparrow$	r=20 $\uparrow$	mAP $\uparrow$	mINP $\uparrow$
Lba [15]	ICCV21	46.38	65.29	72.23	79.41	30.69	-	25.00	54.90	51.87	61.75	27.07	-
AuxNet [21]	TIFS24	51.10	-	-	-	46.00	-	63.60	79.89	85.25	88.31	61.07	-
CAJ [14]	ICCV21	56.59	73.49	79.52	84.05	41.49	-	40.49	66.79	73.32	81.16	41.46	-
CLIP-ReID [51]	AAAI23	58.40	73.20	79.80	-	45.30	-	49.00	73.00	81.20	-	50.40	-
TF-CLIP [22]	AAAI24	62.30	76.20	81.60	-	47.50	-	49.40	76.80	83.70	-	51.90	-
DSAF [47]	TMM25	62.67	75.74	81.17	85.71	49.00	24.93	68.01	85.63	89.08	91.38	65.07	43.30
MITML [19]	CVPR22	63.74	76.90	81.72	86.28	45.31	-	49.07	67.90	75.37	81.53	45.50	-
DNS [16]	ECCV24	64.40	76.85	82.00	<u>86.30</u>	50.68	<u>25.94</u>	<u>69.35</u>	<u>86.21</u>	<u>90.23</u>	<u>92.34</u>	65.93	<u>43.98</u>
SGIEL [17]	CVPR23	67.65	80.30	84.73	-	52.30	-	-	-	-	-	-	-
VLD [23]	TIFS25	<u>74.30</u>	<u>85.00</u>	<u>89.30</u>	-	<u>61.80</u>	-	66.70	85.80	89.90	-	<u>66.00</u>	-
V-DPPT (Ours)	-	<b>58.33</b>	<b>73.12</b>	<b>79.01</b>	<b>83.94</b>	<b>44.99</b>	<b>21.10</b>	<b>52.11</b>	<b>73.37</b>	<b>79.50</b>	<b>86.21</b>	<b>50.70</b>	<b>33.71</b>
$\Delta$	-	15.97	11.88	10.29	2.36	16.81	4.84	17.24	12.84	10.73	6.13	15.30	10.27

TABLE VI

EVALUATION OF OUR V-DPPT UNDER EI AND ES PROTOCOL. THE UPPER PART OF THE TABLE IS UNDER ES, WHILE THE LOWER PART IS UNDER EI. NOTE THAT AS ONLY ONE DATASET IS AVAILABLE DURING TRAINING, WE SPLIT THE CAMERA FOLLOWING THE CI TO ACHIEVE EI, AND THEN DIRECTLY TEST ON THE OTHER DATASET. H AND B DENOTE HITSZ-VCM AND BUPTCAMPUS DATASETS, RESPECTIVELY. THE UPPER PART METHODS ADOPT CENTRALIZED TRAINING, WHILE OUR PROPOSED DPPT ADOPTS DECENTRALIZED TRAINING. THE UNDERLINED AND BOLD INDICATE THE BEST RESULTS FOR BOTH PROTOCOLS, RESPECTIVELY. THE LEFT OF  $\rightarrow$  INDICATES SEEN ENTITIES, AND THE RIGHT IS THE UNSEEN ENTITY.

Methods	Venue	H [19] $\rightarrow$ B [21] (Video)						B [21] $\rightarrow$ H [19] (Video)					
		r=1 $\uparrow$	r=5 $\uparrow$	r=10 $\uparrow$	r=20 $\uparrow$	mAP $\uparrow$	mINP $\uparrow$	r=1 $\uparrow$	r=5 $\uparrow$	r=10 $\uparrow$	r=20 $\uparrow$	mAP $\uparrow$	mINP $\uparrow$
DNS [16]	ECCV24	10.73	22.41	30.08	39.27	13.28	9.76	26.51	44.94	63.62	61.85	14.32	2.11
DSAF [47]	TMM25	12.07	23.75	30.08	38.12	13.35	8.67	29.41	47.53	55.96	64.33	15.36	1.97
VLD [23]	TIFS25	<u>19.35</u>	<u>37.36</u>	<u>46.74</u>	<u>53.64</u>	<u>21.15</u>	<u>13.12</u>	<u>40.84</u>	<u>60.47</u>	<u>68.19</u>	<u>75.92</u>	<u>28.67</u>	<u>8.17</u>
V-DPPT	-	<b>19.54</b>	<b>32.95</b>	<b>41.00</b>	<b>50.00</b>	<b>20.11</b>	<b>13.19</b>	<b>23.84</b>	<b>40.60</b>	<b>49.45</b>	<b>57.85</b>	<b>12.56</b>	<b>1.68</b>

which aligns with the trend observed in image-based datasets. In fact, the VLD introduces text modality as auxiliary and employs the CLIP vision encoder (ViT-B-16) and text encoder, making it significantly more complex than other methods. After excluding the VLD method, our DPPT shows only a 9.32% rank-1 accuracy gap compared to the second-best method SGIEL on the HITSZ-VCM dataset. This observation further underscores the potential of decentralized training in advancing practical applications of VI-ReID.

**Evaluation on the ES Protocol.** We reproduced several existing methods to assess their generalization ability under the ES protocol, as shown in Tab. VI. Given that only two public

datasets are available, we performed centralized training on one dataset and tested on the other, which serves as an unseen domain. The limited dataset availability makes the EI protocol infeasible due to the lack of inter-entity collaboration. To overcome this, we follow the CI protocol during the training, where data is partitioned by camera, then directly test on the other unseen dataset. This is more challenging than the image-level EI protocol. As illustrated in Tab. VI, our decentralized method achieves significant performance in the H $\rightarrow$ B setting. In the B $\rightarrow$ H setting, it performs comparably to DNS and DSAF. While a noticeable gap remains between our DPPT and VLD, it is important to highlight that ours is a baseline

TABLE VII  
ABLATION STUDIES ON SYSU-MM01 AND LLCM DATASETS. THE  
THE LAST ROW SHOWS OUR FINAL CHOSEN SETTING.

Settings	SYSU-MM01 [2] (Image)			LLCM [3] (Image)		
	r=1 $\uparrow$	mAP $\uparrow$	mINP $\uparrow$	r=1 $\uparrow$	mAP $\uparrow$	mINP $\uparrow$
B	27.51	29.98	19.79	26.24	33.52	30.24
B+CA	39.47	39.78	26.95	30.47	37.30	34.09
B+gray	35.25	36.16	24.03	29.33	36.29	33.06
B+CA+ $\mathcal{L}_{mrb}$	<b>51.27</b>	<b>49.29</b>	<b>34.47</b>	<b>34.69</b>	<b>41.91</b>	<b>38.48</b>

TABLE VIII  
ABLATION STUDIES ON HITSZ-VCM AND BUPTCAMPUS  
DATASETS. THE LAST ROW SHOWS OUR FINAL CHOSEN SETTING.

Settings	HITSZ-VCM [19] (Video)			BUPTCampus [21] (Video)		
	r=1 $\uparrow$	mAP $\uparrow$	mINP $\uparrow$	r=1 $\uparrow$	mAP $\uparrow$	mINP $\uparrow$
B	52.51	39.27	15.89	39.66	39.70	27.17
B+CA	52.36	39.06	16.31	41.00	40.26	27.27
B+CA+ $\mathcal{L}_{mrb}$	<b>58.33</b>	<b>44.99</b>	<b>21.10</b>	<b>52.11</b>	<b>50.70</b>	<b>33.71</b>

approach without additional strategies or modules. Notably, in the H $\rightarrow$ B setting, where the training data is larger, VLD suffers from overfitting, resulting in performance on par with our DPPT method.

### E. Ablation Study

**Effectiveness of Each Component.** To evaluate the contribution of each component, we first conduct a series of ablation experiments on SYSU-MM01 [2] and LLCM [3] datasets under the CI protocol. The results are shown in Tab. VII. Baseline denotes that we employ the FedAvg [24] to train the ResNet-50 and optimized by  $\mathcal{L}_{id}$  and  $\mathcal{L}_{cir}$ . Compared with the grayscale, Channel Augmentation (CA) [14] brings a superior improvement. This is because CA preserves original information by randomly mapping one channel to the other two, whereas grayscale discards valuable color information crucial for identity discrimination. Subsequently, our proposed  $\mathcal{L}_{mrb}$ , mitigates the identity missing and domain shift issues by correct the center point across clients, thus further improves the performance. The ablation study under EI is shown in Tab. IV, showing consistent improvement by adding each component. Then, we conduct ablation experiments on two public video datasets, *i.e.*, HITSZ-VCM [19] and BUPTCampus [21] under the CI protocol. The results are reported in Tab. VIII. Unlike in image-based VI-ReID, the CA module brings little improvement in the video setting. A potential reason is that video-based VI-ReID takes sequences of pedestrian frames as input, requiring the model to first learn a temporal-invariant representation to preserve identity information before it can effectively address cross-modality discrepancies. However, our proposed MRB still yields significant performance gains, as it effectively mitigates domain shift and identity missing issues. Regardless of whether the input is image or video data, our proposed MRB consistently enhances retrieval performance, demonstrating its effectiveness and adaptability.

**Hyper-Parameter Ablation.** The hyper-parameter ablation of  $\lambda$  and Top  $K$  is as shown in Fig. 5(a) and (b).  $\lambda$  is used

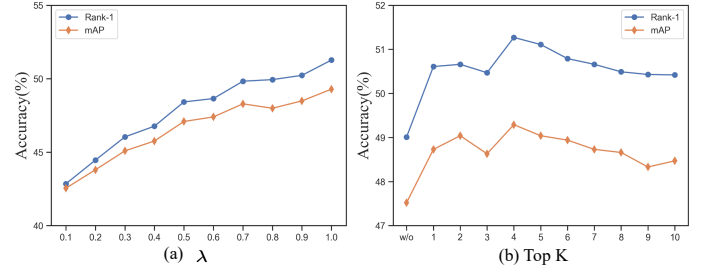


Fig. 5. The effect of hyperparameter  $\lambda$  and  $K$  on the SYSU-MM01 dataset.

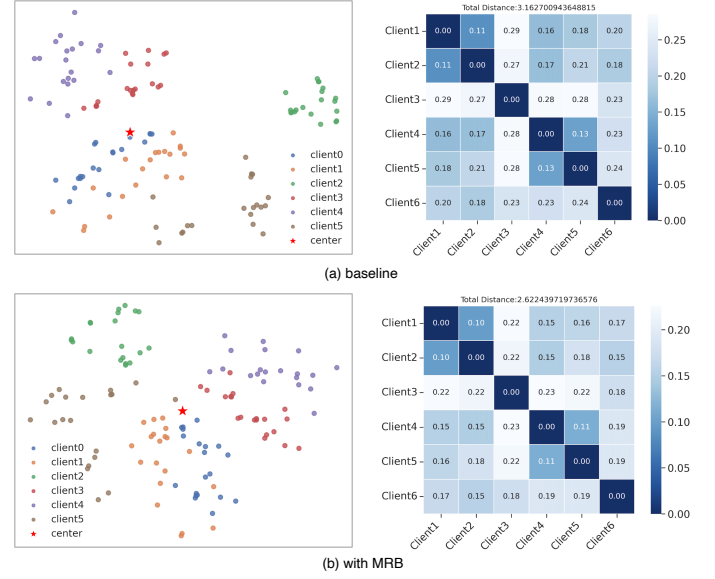


Fig. 6. The ablation study of the proposed MRB. The values in the matrix represent the Euclidean distances between the pedestrian feature centers of two clients. A smaller distance indicates less gap between clients.

to control the MRB. As  $\lambda$  increases, both rank-1 and mAP accuracy consistently improve, reaching the best performance when  $\lambda = 1.0$ . The potential reason is that identity missing and domain shift are two major challenges in decentralized VI-ReID training. Our MRB is specifically designed to mitigate these issues by learn consistent representation across clients. Therefore, increasing  $\lambda$  strengthens the effect of MRB, leading to significant improvements in retrieval accuracy.  $K$  controls the number of features used to compute the client identity center in our MRB. It can be observed that increasing  $K$  from 1 to 4 leads to consistent improvements in both rank-1 and mAP accuracy, with the best performance achieved at  $K = 4$ . This is because the computed identity center can be viewed as a robust representation of pedestrians within each client. Through the optimization of our MRB, this representation effectively alleviates the domain shift issue. However, when  $K$  continues to increase beyond 4, retrieval performance begins to decline. The client center is affected by features that are distant from the true global representation, introducing bias and hindering the alignment of optimization across different clients toward a same target. Therefore, we set  $K = 4$  as the optimal value.

**Effectiveness of MRB.** To evaluate the effectiveness of



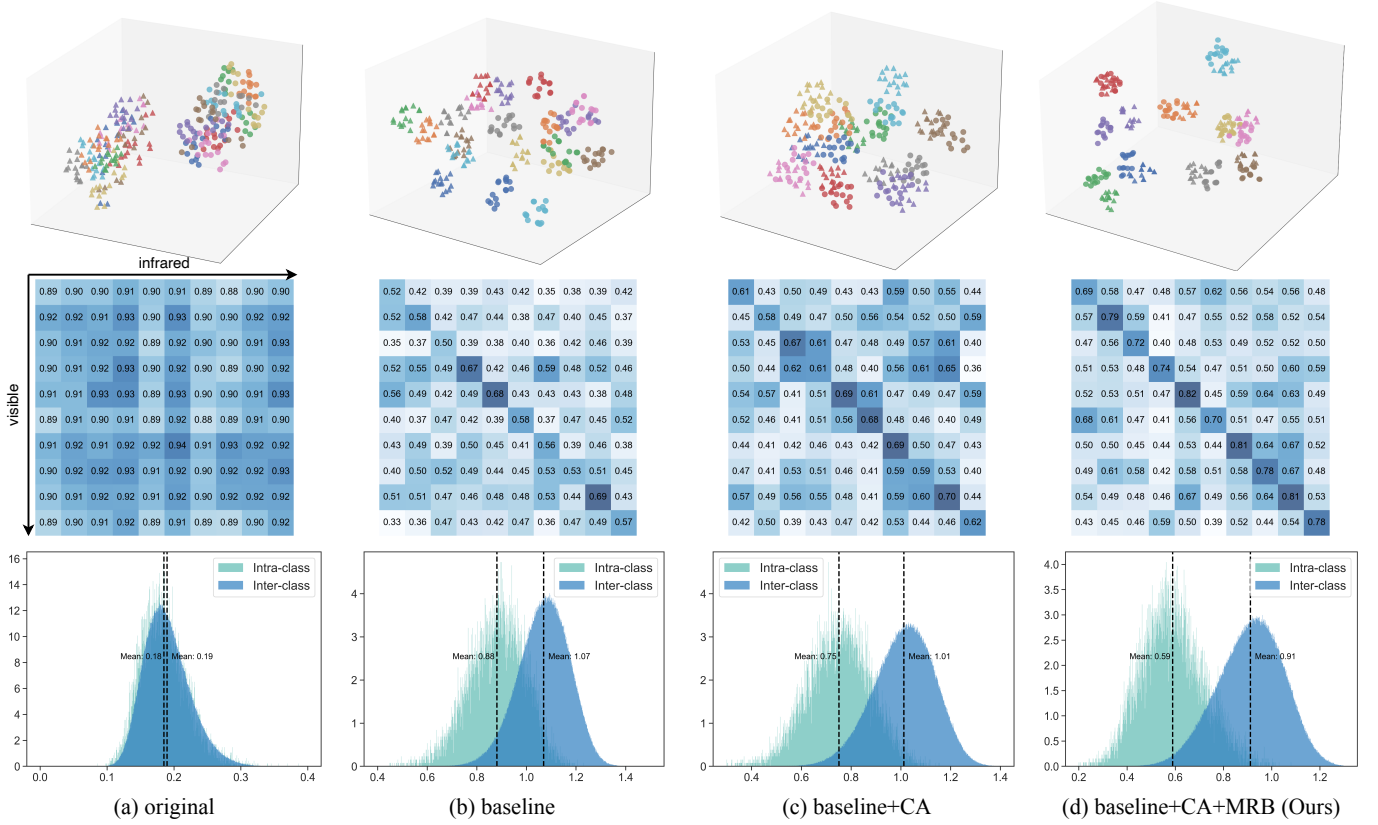


Fig. 7. t-SNE, cosine similarity and intra-inter distances visualization of each component. The circles and triangles denote the visible and infrared modality, respectively. Different colors denote different identities. Each entry in the cosine similarity represents the average similarity between the features of one identity in the visible modality and another identity in the infrared modality. The values range from 0 to 1, where higher diagonal values indicate stronger cross-modality identity consistency.

the proposed MRB, we perform t-SNE visualizations on the SYSU-MM01 dataset by randomly sampling 20 images of the same identity from each client. The results are shown in Fig. 6. Each entry in the matrix indicates the Euclidean distance between the pedestrian feature centers of two clients, where smaller values indicate less domain shift. In the baseline setting, the features from certain clients (e.g., green and gray) are noticeably distant from those of other clients as well as from the global feature center, indicating a severe domain shift issue. In contrast, with the introduction of MRB, the features from all clients are better aligned toward the center. The feature distributions across different clients (indicated by different colors) appear more uniform and are closer to the global center. In addition, the total Euclidean distance of all clients decreases from 3.16 to 2.62. These observations indicate that the domain shift issue is effectively mitigated. Therefore, the proposed MRB substantially mitigates the cross-modality discrepancy, resulting in notable gains in retrieval performance.

#### F. Visualization and Discussion

**Visualization.** To demonstrate the effectiveness of each component, we visualize the distribution of learned features by t-SNE [52], cosine similarity, and intra-class and inter-class distances, as shown in Fig. 7. In Fig. 7(a), the features extracted by the ResNet-50 pretrained on ImageNet-

1k exhibit a large separation between visible and infrared modalities in the t-SNE visualization. The cosine similarity matrix also shows little distinction between diagonal and off-diagonal values, and the difference between intra-class and inter-class distances is minimal. These observations indicate that the cross-modality gap is huge and the identity discriminability of model is very poor. Subsequently, with our baseline, as illustrated in Fig. 7(b), features belonging to the same identity (denoted by color) are more tightly clustered, the diagonal entries in the similarity matrix become more distinguishable, and the gap between intra-class and inter-class distances increases. This suggests that the baseline effectively reduces intra-modality variations. However, it still struggles to eliminate the cross-modality gap, resulting in limited improvement in identity discriminability. Then, by introducing the CA module (Fig. 7(c)), the modality discrepancy is further alleviated. In the t-SNE visualization, features of the same identity across modalities are more aligned, the contrast of diagonal values in the similarity matrix improves, and the intra-inter class distance gap becomes larger. Nevertheless, due to the domain shift issue, identity separability remains suboptimal. Specifically, the inter-class clusters are not well-separated in the t-SNE plot, the diagonal vs. off-diagonal contrast in the similarity matrix is still limited, and the mean intra-class distance remains relatively high. Finally, with the

TABLE IX

ROBUSTNESS EXPERIMENTS ON THE SYSU-MM01 AND LLCM DATASETS. THE CLEAN SETTING REFERS TO THE STANDARD, UNPERTURBED INPUT. FGSM, PGD, BIM, MIFGSM, AND TIFGSM ARE CLASSIC ADVERSARIAL ATTACK METHODS USED TO EVALUATE MODEL VULNERABILITY. CORRUPTION SIMULATES REAL-WORLD CONDITIONS SUCH AS RAIN, SNOW, FOG, *etc.* ↓ DENOTES THE ACCURACY DEGRADATION CAUSED BY ATTACKS.

Attack	SYSU-MM01 [2]				LLCM [3]			
	DNS [16]		Ours		DNS [16]		Ours	
	r=1 ↑	mAP ↑	r=1 ↑	mAP ↑	r=1 ↑	mAP ↑	r=1 ↑	mAP ↑
Clean	77.27	74.35	51.27	49.29	57.45	64.11	34.69	41.91
FGSM [53]	10.82	10.73	11.35	11.52	17.17	21.91	13.88	17.54
↓	85.9%	85.6%	77.8%	76.6%	70.1%	65.9%	60.0%	58.1%
PGD [54]	10.84	11.27	13.22	13.72	13.15	18.05	13.73	17.70
↓	85.9%	84.8%	74.2%	72.2%	77.1%	71.9%	60.4%	57.8%
BIM [55]	61.23	59.79	38.68	39.05	49.53	57.11	28.70	35.84
↓	20.8%	19.6%	24.6%	20.8%	13.8%	10.9%	17.3%	14.5%
MIFGSM [56]	13.93	13.27	15.90	12.10	16.89	21.75	15.31	19.22
↓	82.0%	82.1%	69.0%	75.5%	70.6%	66.1%	55.9%	54.1%
TIFGSM [57]	11.79	11.61	12.62	12.52	16.13	20.82	13.91	17.63
↓	84.7%	84.4%	75.4%	74.6%	71.9%	67.5%	59.9%	57.9%
Corruption [58]	50.91	36.98	33.50	30.14	33.06	36.54	21.30	25.96
↓	34.1%	50.3%	34.6%	38.9%	42.4%	43.0%	38.6%	38.0%

introduction of our proposed MRB (Fig. 7(d)), these issues are significantly mitigated. Features of the same identity are tightly grouped, and different identities become more clearly separated in the t-SNE. The diagonal values in the similarity matrix are noticeably higher than the off-diagonal entries, and the intra-class distances are further reduced. This demonstrates that MRB effectively addresses the domain shift problem, leading to enhanced identity discriminability and improved retrieval performance.

**Discussion on the robustness.** In practical surveillance systems, adverse weather such as rain, snow, and fog is common and can degrade image quality, making cross-modality retrieval more difficult. At the same time, VI-ReID is widely used in public safety applications and is susceptible to malicious attacks, which may reduce retrieval accuracy or expose sensitive identity information. To address these concerns, we conduct experiments that simulate environmental degradation and evaluate representative adversarial attacks in order to assess robustness and quantify potential privacy risks, as shown in Tab. IX. It can be observed that our decentralized training method only experiences a slightly drop in rank-1 accuracy than the centralized training methods DNS under the BIM attack. For other attacks (i.e., FGSM, PGD, MIFGSM and TIFGSM), our methods exhibit a smaller accuracy drop compared to DNS. It is worth noting that under the clean setting, our method shows a noticeable performance gap compared to DNS. However, under the above four adversarial attacks, our method even outperforms DNS. This improvement may be attributed to the decentralized training strategy, which enables the model to learn diverse feature representations from multiple clients. Such diversity helps mitigate overfitting and enhances the model’s robustness against adversarial perturbations. Furthermore, under simulated real-world scenarios (Corruption), our method demonstrates greater robustness, with less accuracy drop than DNS. These results highlight the practical advantages of decentralized training over centralized approaches, particularly in terms of robustness under adversarial threats and challenging real-world conditions.

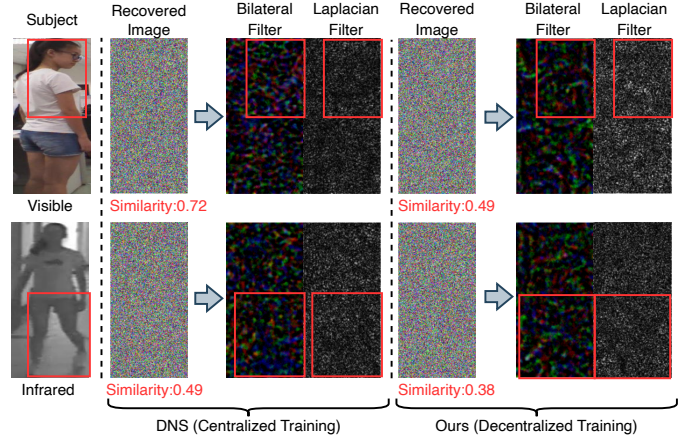


Fig. 8. IDLG [59] gradient inversion visualization. Subject is the target pedestrian image. The recovered image is reconstructed from the subject’s gradients using iDLG. The two images to the right of the recovered image are obtained by applying a bilateral filter and a Laplacian filter, respectively. Similarity is defined as the cosine similarity between the feature vectors of the subject image and the recovered image after being processed by the encoder. It serves as an indicator of how accurately the pedestrian’s attributes have been reconstructed. The value closer to 1 indicates a higher degree of similarity between the two images.

**Discussion on privacy.** To evaluate the potential privacy risks of L2RW+, we utilize iDLG [59], a gradient inversion technique, to reconstruct images that simulate gradient leakage scenarios. We adopt the Adam optimizer with a learning rate of 0.01 and perform 200 iterations. The resulting image is shown as the recovered image in Fig. 8. Due to the high level of noise in the recovered image, it is difficult to visually identify meaningful content. Therefore, we further process the recovered image using a bilateral filter and a Laplacian filter, respectively, as illustrated in Fig. 8. In the results reconstructed using centralized training (DNS), clear local features consistent with the subject image can be observed. Specifically, the head region in the visible image and the leg region in the infrared image are clearly reconstructed. In contrast, under our decentralized training method, such attributes are much less distinguishable. Furthermore, we feed both the reconstructed image and the corresponding subject image into the encoder (consistent with the training setup) and compute their cosine similarity. The results show that the cosine similarities obtained under our decentralized training are consistently lower than those from DNS. This indicates that the reconstructed images are less similar to the original subject images, suggesting that our decentralized training method provides better privacy protection than centralized training. This improvement can be attributed to the nature of the training paradigm: centralized training tends to focus on identity-specific features, whereas decentralized training, influenced by multiple clients, learns more generalized representations, making sensitive attributes harder to visually recover.

**Discussion on the impact of data scale.** Tab. III to Tab. VI reveal a positive correlation between data scale and both the retrieval accuracy and generalization ability of decentralized training. Specifically, as shown in Tab. III and Tab. V, the rank-1 accuracy gap between DPPT and the SOTA centralized

methods decreases with larger training data, in both image and video datasets. Regarding generalization, Tab. IV and Tab. VI show that under larger-scale settings such as  $L + S \rightarrow R$  and  $H \rightarrow B$ , DPPT achieves performance comparable to centralized baselines and even performs best in the  $L + S \rightarrow R$  setting. These results suggest that constructing a larger-scale VI-ReID dataset would be beneficial for advancing decentralized training in this field.

**Limitations.** This work revisits VI-ReID and introduces a decentralized training approach for privacy-preserved VI-ReID. However, under the CI protocol, our method still exhibits a performance gap compared to methods with fully shared data [3], [16], [17], [23], [47]. Moreover, the overall rank-1 accuracy remains relatively low under both the ES and EI protocols, indicating that generalization to unseen environments remains a fundamental challenge for VI-ReID, regardless of whether centralized or decentralized training.

**Future works.** In future work, we plan to extend our research in the following three directions. **1) Improving performance under different protocols.** As our benchmark primarily serves an exploratory purpose, we have demonstrated the feasibility of applying decentralized training to VI-ReID. Our current method does not incorporate additional modules or strategies, which makes it highly adaptable. Moving forward, we aim to explore more advanced techniques to enhance the model's ability to handle cross-modality discrepancies under the CI protocol and to improve its generalization to unseen domains across all protocols. **2) Constructing larger-scale VI-ReID datasets.** Experimental results under all three protocols indicate that the retrieval accuracy and generalization performance of our DPPT approach improve as the training data scale increases. However, existing public datasets are still limited in size compared to the volume of data typically collected in real-world surveillance systems. Therefore, we plan to build a larger-scale VI-ReID dataset to investigate the impact of data scale on decentralized VI-ReID. **3) Removing label information.** Although our current approach achieves promising results in both image- and video-based VI-ReID, it still relies on labeled data. In practice, annotating large-scale surveillance imagery is highly impractical. Thus, after improving the supervised accuracy of our method, we will explore how to perform decentralized VI-ReID in an unsupervised manner. This step is essential for making VI-ReID more applicable in real-world deployments.

## V. CONCLUSION

This paper presents L2RW+, the first privacy-preserved benchmark for VI-ReID, which aims to bring VI-ReID closer to real-world applications. To simulate privacy constraints, we introduce three protocols: camera independence (CI), entity independence (EI), and entity sharing (ES). We also propose the I-DPPT and V-DPPT for image and video data, which addresses challenges under both protocols without compromising data privacy. Extensive experiments across both image- and video-level VI-ReID datasets validate the feasibility and effectiveness of decentralized training under privacy-preserving conditions. Our results further show that decentralized training

exhibits better generalization than centralized training. We also reveal that scaling up the data improves both retrieval accuracy and generalization in decentralized training. These findings demonstrate that privacy-preserved VI-ReID is both effective and practical, and we hope this work inspires future research in privacy-preserved VI-ReID and advances the field.

## REFERENCES

- [1] Y. Jiang, H. Yu, X. Cheng, H. Chen, Z. Sun, and G. Zhao, "From laboratory to real world: A new benchmark towards privacy-preserved visible-infrared person re-identification," in *Proceedings of the Computer Vision and Pattern Recognition Conference*, 2025, pp. 8828–8837.
- [2] A. Wu, W.-S. Zheng, H.-X. Yu, S. Gong, and J. Lai, "Rgb-infrared cross-modality person re-identification," in *Proceedings of the IEEE international conference on computer vision*, 2017, pp. 5380–5389.
- [3] Y. Zhang and H. Wang, "Diverse embedding expansion network and low-light cross-modality benchmark for visible-infrared person re-identification," in *Proceedings of the IEEE/CVF Conference on Computer Vision and Pattern Recognition*, 2023, pp. 2153–2162.
- [4] M. Ye, Z. Wu, C. Chen, and B. Du, "Channel augmentation for visible-infrared re-identification," *IEEE Transactions on Pattern Analysis and Machine Intelligence*, 2023.
- [5] H. Yu, X. Cheng, and W. Peng, "Toplight: Lightweight neural networks with task-oriented pretraining for visible-infrared recognition," in *CVPR*, 2023, pp. 3541–3550.
- [6] H. Yu, X. Cheng, W. Peng, W. Liu, and G. Zhao, "Modality unifying network for visible-infrared person re-identification," in *ICCV*, 2023, pp. 11 185–11 195.
- [7] Y. Zhang, Y. Lu, Y. Yan, H. Wang, and X. Li, "Frequency domain nuances mining for visible-infrared person re-identification," *arXiv preprint arXiv:2401.02162*, 2024.
- [8] K. Ren and L. Zhang, "Implicit discriminative knowledge learning for visible-infrared person re-identification," in *Proceedings of the IEEE/CVF Conference on Computer Vision and Pattern Recognition*, 2024, pp. 393–402.
- [9] Z. Wu and M. Ye, "Unsupervised visible-infrared person re-identification via progressive graph matching and alternate learning," in *CVPR*, 2023, pp. 9548–9558.
- [10] B. Yang, J. Chen, and M. Ye, "Towards grand unified representation learning for unsupervised visible-infrared person re-identification," in *ICCV*, 2023, pp. 11 069–11 079.
- [11] —, "Shallow-deep collaborative learning for unsupervised visible-infrared person re-identification," in *Proceedings of the IEEE/CVF Conference on Computer Vision and Pattern Recognition*, 2024, pp. 16 870–16 879.
- [12] J. Wu, H. Liu, Y. Su, W. Shi, and H. Tang, "Learning concordant attention via target-aware alignment for visible-infrared person re-identification," in *Proceedings of the IEEE/CVF International Conference on Computer Vision*, 2023, pp. 11 122–11 131.
- [13] M. Ye, J. Shen, G. Lin, T. Xiang, L. Shao, and S. C. Hoi, "Deep learning for person re-identification: A survey and outlook," *IEEE transactions on pattern analysis and machine intelligence*, vol. 44, no. 6, pp. 2872–2893, 2021.
- [14] M. Ye, W. Ruan, B. Du, and M. Z. Shou, "Channel augmented joint learning for visible-infrared recognition," in *Proceedings of the IEEE/CVF International Conference on Computer Vision*, 2021, pp. 13 567–13 576.
- [15] H. Park, S. Lee, J. Lee, and B. Ham, "Learning by aligning: Visible-infrared person re-identification using cross-modal correspondences," in *Proceedings of the IEEE/CVF international conference on computer vision*, 2021, pp. 12 046–12 055.
- [16] Y. Jiang, X. Cheng, H. Yu, X. Liu, H. Chen, and G. Zhao, "Domain shifting: A generalized solution for heterogeneous cross-modality person re-identification," in *European Conference on Computer Vision*. Springer, 2025, pp. 289–306.
- [17] J. Feng, A. Wu, and W.-S. Zheng, "Shape-erased feature learning for visible-infrared person re-identification," in *CVPR*, 2023, pp. 22 752–22 761.
- [18] Y. Zhang, Y. Yan, Y. Lu, and H. Wang, "Towards a unified middle modality learning for visible-infrared person re-identification," in *Proceedings of the 29th ACM international conference on multimedia*, 2021, pp. 788–796.



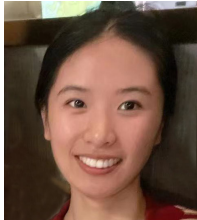
- [19] X. Lin, J. Li, Z. Ma, H. Li, S. Li, K. Xu, G. Lu, and D. Zhang, "Learning modal-invariant and temporal-memory for video-based visible-infrared person re-identification," in *Proceedings of the IEEE/CVF Conference on Computer Vision and Pattern Recognition*, 2022, pp. 20973–20982.
- [20] H. Li, M. Liu, Z. Hu, F. Nie, and Z. Yu, "Intermediary-guided bidirectional spatial-temporal aggregation network for video-based visible-infrared person re-identification," *IEEE Transactions on Circuits and Systems for Video Technology*, vol. 33, no. 9, pp. 4962–4972, 2023.
- [21] Y. Du, C. Lei, Z. Zhao, Y. Dong, and F. Su, "Video-based visible-infrared person re-identification with auxiliary samples," *IEEE Transactions on Information Forensics and Security*, vol. 19, pp. 1313–1325, 2023.
- [22] C. Yu, X. Liu, Y. Wang, P. Zhang, and H. Lu, "Tf-clip: Learning text-free clip for video-based person re-identification," in *Proceedings of the AAAI conference on artificial intelligence*, vol. 38, no. 7, 2024, pp. 6764–6772.
- [23] S. Li, J. Leng, C. Kuang, M. Tan, and X. Gao, "Video-level language-driven video-based visible-infrared person re-identification," *IEEE Transactions on Information Forensics and Security*, 2025.
- [24] B. McMahan, E. Moore, D. Ramage, S. Hampson, and B. A. y Arcas, "Communication-efficient learning of deep networks from decentralized data," in *Artificial intelligence and statistics*. PMLR, 2017, pp. 1273–1282.
- [25] T. Li, A. K. Sahu, M. Zaheer, M. Sanjabi, A. Talwalkar, and V. Smith, "Federated optimization in heterogeneous networks," *Proceedings of Machine learning and systems*, vol. 2, pp. 429–450, 2020.
- [26] Q. Li, B. He, and D. Song, "Model-contrastive federated learning," in *CVPR*, 2021, pp. 10713–10722.
- [27] W. Huang, M. Ye, Z. Shi, H. Li, and B. Du, "Rethinking federated learning with domain shift: A prototype view," in *CVPR*. IEEE, 2023, pp. 16312–16322.
- [28] L. Qu, Y. Zhou, P. P. Liang, Y. Xia, F. Wang, E. Adeli, L. Fei-Fei, and D. Rubin, "Rethinking architecture design for tackling data heterogeneity in federated learning," in *CVPR*, 2022, pp. 10061–10071.
- [29] Z. Qu, X. Li, R. Duan, Y. Liu, B. Tang, and Z. Lu, "Generalized federated learning via sharpness aware minimization," in *International conference on machine learning*. PMLR, 2022, pp. 18250–18280.
- [30] Y. Tan, G. Long, L. Liu, T. Zhou, Q. Lu, J. Jiang, and C. Zhang, "Fedproto: Federated prototype learning across heterogeneous clients," in *AAAI*, vol. 36, no. 8, 2022, pp. 8432–8440.
- [31] W. Huang, M. Ye, and B. Du, "Learn from others and be yourself in heterogeneous federated learning," in *CVPR*, 2022, pp. 10143–10153.
- [32] D. Makhija, X. Han, N. Ho, and J. Ghosh, "Architecture agnostic federated learning for neural networks," in *International Conference on Machine Learning*. PMLR, 2022, pp. 14860–14870.
- [33] M. Ye, X. Fang, B. Du, P. C. Yuen, and D. Tao, "Heterogeneous federated learning: State-of-the-art and research challenges," *ACM Computing Surveys*, vol. 56, no. 3, pp. 1–44, 2023.
- [34] Y. Feng, J. Jiang, M. Tang, R. Jin, and Y. Gao, "Rethinking supervised pre-training for better downstream transferring," *arXiv preprint arXiv:2110.06014*, 2021.
- [35] J. Hu, L. Qi, J. Zhang, and Y. Shi, "Domain generalization via inter-domain alignment and intra-domain expansion," *Pattern Recognition*, vol. 146, p. 110029, 2024.
- [36] A. Ballas and C. Diou, "Multi-scale and multi-layer contrastive learning for domain generalization," *IEEE Transactions on Artificial Intelligence*, 2024.
- [37] H. Li, S. J. Pan, S. Wang, and A. C. Kot, "Domain generalization with adversarial feature learning," in *Proceedings of the IEEE conference on computer vision and pattern recognition*, 2018, pp. 5400–5409.
- [38] Y. Li, X. Tian, M. Gong, Y. Liu, T. Liu, K. Zhang, and D. Tao, "Deep domain generalization via conditional invariant adversarial networks," in *Proceedings of the European conference on computer vision (ECCV)*, 2018, pp. 624–639.
- [39] A. Dayal, V. KB, L. R. Cenkeramaddi, C. Mohan, A. Kumar, and V. N. Balasubramanian, "Madg: margin-based adversarial learning for domain generalization," *Advances in Neural Information Processing Systems*, vol. 36, 2024.
- [40] D. Mahajan, S. Tople, and A. Sharma, "Domain generalization using causal matching," in *International conference on machine learning*. PMLR, 2021, pp. 7313–7324.
- [41] K. Ahuja, E. Caballero, D. Zhang, J.-C. Gagnon-Audet, Y. Bengio, I. Mitliagkas, and I. Rish, "Invariance principle meets information bottleneck for out-of-distribution generalization," *Advances in Neural Information Processing Systems*, vol. 34, pp. 3438–3450, 2021.
- [42] S. Sun, S. Zhi, Q. Liao, J. Heikkilä, and L. Liu, "Unbiased scene graph generation via two-stage causal modeling," *IEEE Transactions on Pattern Analysis and Machine Intelligence*, vol. 45, no. 10, pp. 12562–12580, 2023.
- [43] V. Vapnik, "Principles of risk minimization for learning theory," *Advances in neural information processing systems*, vol. 4, 1991.
- [44] D. T. Nguyen, H. G. Hong, K. W. Kim, and K. R. Park, "Person recognition system based on a combination of body images from visible light and thermal cameras," *Sensors*, vol. 17, no. 3, p. 605, 2017.
- [45] J. Wang, Q. Liu, H. Liang, G. Joshi, and H. V. Poor, "Tackling the objective inconsistency problem in heterogeneous federated optimization," *Advances in neural information processing systems*, vol. 33, pp. 7611–7623, 2020.
- [46] L. Qiu, S. Chen, Y. Yan, J.-H. Xue, D.-H. Wang, and S. Zhu, "High-order structure based middle-feature learning for visible-infrared person re-identification," in *Proceedings of the AAAI Conference on Artificial Intelligence*, vol. 38, no. 5, 2024, pp. 4596–4604.
- [47] Y. Jiang, X. Cheng, H. Yu, X. Liu, H. Chen, and G. Zhao, "Dsaf: Dual space alignment framework for visible-infrared person re-identification," *IEEE Transactions on Multimedia*, 2025.
- [48] K. He, X. Zhang, S. Ren, and J. Sun, "Deep residual learning for image recognition," in *Proceedings of the IEEE conference on computer vision and pattern recognition*, 2016, pp. 770–778.
- [49] J. Deng, W. Dong, R. Socher, L.-J. Li, K. Li, and L. Fei-Fei, "Imagenet: A large-scale hierarchical image database," in *2009 IEEE conference on computer vision and pattern recognition*. Ieee, 2009, pp. 248–255.
- [50] L. N. Smith and N. Topin, "Super-convergence: Very fast training of neural networks using large learning rates," in *Artificial intelligence and machine learning for multi-domain operations applications*, vol. 11006. SPIE, 2019, pp. 369–386.
- [51] S. Li, L. Sun, and Q. Li, "Clip-reid: exploiting vision-language model for image re-identification without concrete text labels," in *Proceedings of the AAAI conference on artificial intelligence*, vol. 37, no. 1, 2023, pp. 1405–1413.
- [52] L. Van der Maaten and G. Hinton, "Visualizing data using t-sne," *Journal of machine learning research*, vol. 9, no. 11, 2008.
- [53] I. J. Goodfellow, J. Shlens, and C. Szegedy, "Explaining and harnessing adversarial examples," *arXiv preprint arXiv:1412.6572*, 2014.
- [54] A. Madry, A. Makelov, L. Schmidt, D. Tsipras, and A. Vladu, "Towards deep learning models resistant to adversarial attacks," *arXiv preprint arXiv:1706.06083*, 2017.
- [55] A. Kurakin, I. J. Goodfellow, and S. Bengio, "Adversarial examples in the physical world," in *Artificial intelligence safety and security*. Chapman and Hall/CRC, 2018, pp. 99–112.
- [56] Y. Dong, F. Liao, T. Pang, H. Su, J. Zhu, X. Hu, and J. Li, "Boosting adversarial attacks with momentum," in *Proceedings of the IEEE conference on computer vision and pattern recognition*, 2018, pp. 9185–9193.
- [57] Y. Dong, T. Pang, H. Su, and J. Zhu, "Evading defenses to transferable adversarial examples by translation-invariant attacks," in *Proceedings of the IEEE/CVF conference on computer vision and pattern recognition*, 2019, pp. 4312–4321.
- [58] M. Chen, Z. Wang, and F. Zheng, "Benchmarks for corruption invariant person re-identification," *arXiv preprint arXiv:2111.00880*, 2021.
- [59] B. Zhao, K. R. Mopuri, and H. Bilen, "idlg: Improved deep leakage from gradients," *arXiv preprint arXiv:2001.02610*, 2020.



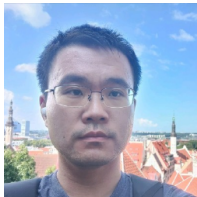
**Yan Jiang** received the B.E. and M.S. degrees from Nanjing University of Information Science and Technology in 2022 and 2025, respectively. He is currently pursuing his Ph.D. degree in computer science from University of Oulu, Finland. His research interests include cross-modality person re-identification, rPPG, and face editing and generation.



**Hao Yu** is currently a PhD student at the University of Oulu, Finland. He previously earned his master's degree from NUIST. His research interests focus on facial attribute analysis and privacy protection.



**Mengting Wei** is currently a PhD student at the University of Oulu, Finland. She previously earned her master's degree from Southeast University and completed her bachelor's degree at Hebei University of Technology. Her research interests focus on facial expression analysis, face generation and editing.



**Zhaodong Sun** received the B.E. degree from the University of Electronic Science and Technology of China in 2018, the MSc degree from the Swiss Federal Institute of Technology Lausanne in 2020, and the doctoral degree from the University of Oulu in 2024. He is currently a lecturer at the Nanjing University of Information Science and Technology. His research interests include computer vision, biomedical signal processing, remote physiological measurement, and affective computing.



**Haoyu Chen** received his Ph.D degree in Computer Science and Engineering from the University of Oulu, Finland, in 2022. He is currently a Tenure Track Assistant Professor with CMVS and Academy Research Fellow, at the University of Oulu, Finland. He has actively chaired workshops and challenges at various conferences, including HHAI 2024, IJCAI 2023, and IJCAI 2024. His work on gesture recognition has received notable recognition, including the second prize of the IEEE Finland Jt. Chapter SP/CAS Best Paper Award, the 2nd place in the

Action Recognition Track of the ECCV 2020 VIPriors Challenges, etc. His research interests include human behavior analysis, hybrid intelligence, and emotion AI.



**Guoying Zhao** received the Ph.D. degree in computer science from the Chinese Academy of Sciences, Beijing, China, in 2005. She is currently an Academy Professor and full Professor (tenured in 2017) with University of Oulu. She is also a visiting professor with Aalto University. She is a member of Academia Europaea, a member of Finnish Academy of Sciences and Letters, IEEE Fellow, IAPR Fellow and ELLIS Fellow. She has authored or co-authored more than 330 papers in journals and conferences with 28,070+ citations in Google Scholar and h-index 83. She is panel chair for FG 2023, publicity chair of 22nd Scandinavian Conference on Image Analysis (SCIA 2023), was co-program chair for ACM International Conference on Multimodal Interaction (ICMI 2021), co-publicity chair for FG 2018, and has served as area chairs for several conferences and was/is associate editor for IEEE Trans. on Multimedia, Pattern Recognition, IEEE Trans. on Circuits and Systems for Video Technology, Image and Vision Computing and Frontiers in Psychology Journals. Her current research interests include image and video descriptors, facial-expression and micro-expression recognition, emotional gesture analysis, affective computing, and biometrics. Her research has been reported by Finnish TV programs, newspapers and MIT Technology Review.



**Xu Cheng** received the B.E. and M.E. degrees in information engineering from the Taiyuan University of Technology, Taiyuan, in 2007 and 2010, respectively, and the Ph.D. degree in information and communication engineering from Southeast University, Nanjing, China, in 2015. He is currently a full Professor with the School of Computer Science, Nanjing University of Information Science and Technology, China. His research interests include computer vision, object tracking, multi-modal information processing and pattern recognition.